APS physics

CHORUS

This is the accepted manuscript made available via CHORUS. The article has been published as:

Spin mixing and protection of ferromagnetism in a spinor dipolar condensate

S. Lepoutre, K. Kechadi, B. Naylor, B. Zhu, L. Gabardos, L. Isaev, P. Pedri, A. M. Rey, L. Vernac, and B. Laburthe-Tolra

Phys. Rev. A **97**, 023610 — Published 6 February 2018

DOI: 10.1103/PhysRevA.97.023610

Spin mixing and protection of ferromagnetism in a spinor dipolar condensate

S. Lepoutre[1,2], K. Kechadi[1,2], B. Naylor[1,2], B. Zhu[3], L. Gabardos[1,2],
L. Isaev[3], P. Pedri[1,2], A. M. Rey[3], L. Vernac[1,2], B. Laburthe-Tolra[2,1].
[1] *Université Paris 13, Sorbonne Paris Cité, Laboratoire de Physique des Lasers, F-93430, Villetaneuse, France*
[2] *CNRS, UMR 7538, LPL, F-93430, Villetaneuse, France*
[3] *JILA, NIST and Department of Physics, University of Colorado, Boulder, USA*
(Dated: January 23, 2018)

We study spin mixing dynamics in a chromium dipolar Bose-Einstein Condensate, after tilting the atomic spins by an angle θ with respect to the magnetic field. Spin mixing is triggered by dipolar coupling, but, once dynamics has started, it is mostly driven by contact interactions. For the particular case $\theta = \pi/2$, an external spin-orbit coupling term induced by a magnetic gradient is required to enable the dynamics. Then the initial ferromagnetic character of the gas is locally preserved, an unexpected feature that we attribute to large spin-dependent contact interactions.

For spin systems, insight on their collective behaviour can be gained from observations following a rotation of the individual spins initially oriented along the external magnetic field. Deviation from an overall precession of the spins at the Larmor frequency may reveal interparticle interactions. This generic problem is encountered for example in Nuclear Magnetic Resonance, where dipole-dipole interactions (DDIs) is a source of decoherence [1], and thus have to be reduced to obtain long coherence lifetimes of nuclear spins [2]. Similar cancellation of DDIs has also been demonstrated in the case of electrons in semiconductors [3], or for impurity centers in a solid [4].

On the contrary, interaction-induced modification of the mere precession can be desired, as it leads to interesting phenomena. For example DDIs between ultracold molecules in an optical lattice were evidenced this way [5]. For spinor quantum gases [6], i.e. quantum degenerate gases with a spin degrees of freedom, tilting the spins by an angle θ with respect to the magnetic field (see Fig. 1a)) has lead to observation of spontaneous pattern formation due to instabilities driven by DDIs [7, 8] or antiferromagnetic contact interaction [9]. Dipolar spin systems could display beyond mean field physics for angles θ close to $\pi/2$ [10]. Here we rotate the spins of a $s = 3$ ^{52}Cr BEC, and study how spin dynamics develops as an interplay between contact interactions, DDIs, and magnetic field gradients (MGs). One unexpected outcome is that strong spin-dependent contact interactions favor the persistence of ferromagnetic textures (see Fig. 1b)), and seem to slow down beyond mean-field effects.

Compared to alkaline spinor gases, a ^{52}Cr BEC offers two key differences: spin dependent contact interactions are significantly larger [11], and DDIs are 36 times larger. After rotation from an initially polarized BEC in $s = 3, m_s = -3$, atoms are in a stretched (ferromagnetic) state corresponding to a well-defined molecular potential. Starting from this initial state, no spin dynamics can develop under the influence of contact interactions (in contrast with [12], where a non-ferromagnetic initial state was prepared), which display $SU(2)$ symmetry and preserve the total spin. On the other hand, DDIs or MGs,

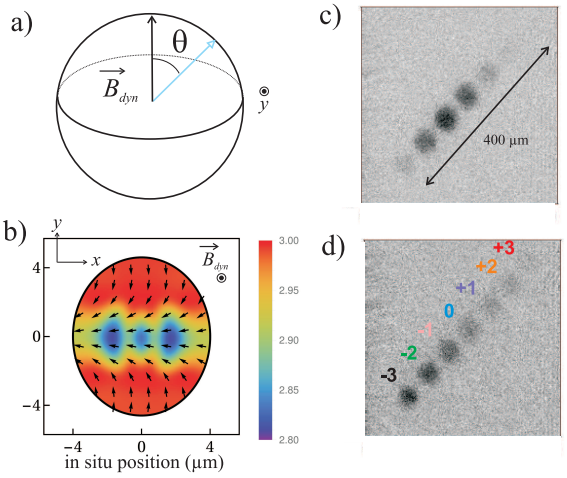

FIG. 1. Principle of the experiment. a) The spins of atoms in a polarized $s = 3$ ^{52}Cr BEC are rotated at $t = 0$, and make an angle θ with respect to the external magnetic field, $\boldsymbol{B}_{\rm dyn}$. b) After a variable time $t_{\rm dyn}$ spins point in different directions (shown by arrows) but have a length almost constant (see color code). The figure is a result of our Gross Pitaevskii simulation for $t_{\rm dyn} = 5$ ms. Right: Absorption imaging after a Stern Gerlach separation allows to measure populations in the seven spin components. Pictures show the seven separated clouds for $\theta = \pi/2$ and the magnetic field configuration of Fig. 3. c) $t_{\rm dyn} = 0.1$ ms. d) $t_{\rm dyn} = 5$ ms.

which convey spin-orbit coupling, can trigger spin mixing. For example, in the mean-field approximation, the dipoles which precess around the external magnetic field create an effective dipolar magnetic field [13], and DDIs result in precession of the spins around this dipolar field. This triggers spin dynamics, unless $\theta = \pi/2$, in which case the dipolar field is parallel to the spins.

Experimentally, we find that DDIs do trigger spin dynamics, even when we best suppress MGs, for $\theta \neq \pi/2$. However, spin dynamics is strongly suppressed for $\theta = \pi/2$ without MGs. For $\theta \approx \pi/2$, we recover spin dynamics by applying MGs, and find that dynamics preserves the initial ferromagnetic character of the BEC. We attribute this unexpected effect to large spin-dependent contact interactions: depolarization is inhibited by an energy gap $\propto 4\pi\hbar^2 n(a_6 - a_4)/M$ (with M the atomic

mass, n the density, and a_S the scattering length associated to the molecular potential S), favouring persistence of locally fully magnetized classical states. We confirm this phenomenon by measuring the norm of the collective spin during dynamics.

The starting point of our experiments is a polarized ^{52}Cr BEC produced in a crossed dipole trap [11], with typically 4×10^4 atoms polarized in the minimal Zeeman energy state $m_s=-3$. Trap frequencies are $\omega_{x,y,z}=2\pi\times(298,245,210)$ Hz, with 5% uncertainty, Oy being the vertical axis. The atomic spins are aligned along an external magnetic field noted $\boldsymbol{B}_{\rm dyn}$, whose average amplitude B_0 is in the $150-200$ mG range, and whose average direction $\hat{u}_B$ is in the horizontal xz plane. $\boldsymbol{B}_{\rm dyn}$ is maintained constant during the whole dynamics. The dynamics is initiated at $t=0$ by a resonant radio-frequency pulse, at the Larmor frequency $f_L=g\mu_B B_0$ ($g=2$ is the Landé factor, μ_B the Bohr magneton), and a Rabi frequency equal to 50 kHz; it rotates all spins by an angle θ, so that $\boldsymbol{s}_{t=0^+}=\cos(\theta)\hat{u}_B+\sin(\theta)\hat{u}_\perp$, ($\hat{u}_\perp\perp(\hat{u}_B,\hat{u}_y)$, see Fig. 1a)). We let the system evolve for a duration $t_{\rm dyn}$. We then switch the optical trap off and spatially separate the 7 spin components during a time of flight of 5 ms, using a Stern Gerlach (SG) technique (see Fig. 1c)d)).Spin populations measured after SG correspond to a projective measurement along $\hat{u}_B$ (see Appendix). From absorption pictures as those shown in Fig. 1c)d), we obtain populations N_{m_s} of all seven spin components (for details on detectivity calibration see Appendix). We then compute the total population $N_{tot}=\sum_{m_s}N_{m_s}$ and fractional populations $p_{m_s}=N_{m_s}/N_{tot}$. We also measured the 3D spatial dependance of $\boldsymbol{B}_{\rm dyn}$, and obtained $|\boldsymbol{B}_{\rm dyn}|=B_0+\boldsymbol{b}.\boldsymbol{r}$ (see Appendix).

Figure 2 displays temporal evolution of p_{m_s} when we best cancel MGs. There is almost no spin mixing dynamics in the case $\theta=\pi/2$ as shown by Fig. 2 a). In absence of MGs, this is expected from the mean-field point of view [13]. On the other hand, spin models do predict beyond mean field dynamics at $\theta=\pi/2$ [10], over a time scale $\simeq10$ ms for our atomic distribution. Simulations of our BEC system based on the Truncated Wigner Approximation [14] indicate that the gap associated to spin-dependent short range interactions delay the onset of beyond mean field corrections.

In contrast, spin mixing dynamics is obtained for a rotation by $\theta=\pi/4$ when MGs are best cancelled (see Fig. 2 b)). The occurrence of spin dynamics in absence of MGs is an experimental signature of DDIs, which break spin rotational symmetry, contrarily to $SU(2)$ symmetric contact or Heisenberg spin-spin interactions. The demonstration of this genuine dipolar dynamics in a BEC is the first main result of this paper.

Figure 3 shows evolution of p_{m_s} for $\theta=\pi/2$ in a case where MGs are not minimized, contrarily to Fig. 2 a). Then a significant dynamics is observed. We find that the general trend is that larger MGs lead to faster spin dynamics (see Appendix). Besides we find a significant decrease of N_{tot} in a few ms, which we attribute to dipolar relaxation collisions [15]. Losses due to dipolar relaxation are more important at $\theta=\pi/2$ compared to $\theta=\pi/4$ due to the larger spin rotation.

The ensemble of results shown in figures 2 and 3 demonstrate the sensitivity of the dynamics not only to the external magnetic field configuration, but as well to the initial preparation (angle θ). In order to understand the influence of these different parameters, and the role played by the different interactions, we have developed a three dimensional spinorial Gross-Pitaevskii (GP) simulation. The seven components of $\boldsymbol{\Psi}$, the spinor describing the condensate field, obey the equations $i\hbar\frac{\partial\Psi_m}{\partial t}=\frac{\delta(H-i\Gamma)}{\delta\Psi_m^*}$, with:

$$
\begin{aligned}
H-i\Gamma=&\int d^3\mathbf{r}\Big(\boldsymbol{\Psi}(\mathbf{r})^\dagger\hat{H}_0\boldsymbol{\Psi}(\mathbf{r})+\mu_B g\,|\boldsymbol{B}_{\rm dyn}|\,S^Z(\mathbf{r})+\frac{c_0}{2}|n(\mathbf{r})|^2\Big)\\
&+\int d^3\mathbf{r}\Big(\frac{c_1}{2}|\mathbf{S}(\mathbf{r})|^2+\frac{c_2}{2}|A_{00}(\mathbf{r})|^2+\frac{c_3}{2}\sum_{M=-2}^{2}|A_{2M_S}(\mathbf{r})|^2\Big)\\
&-\frac{c_{dd}}{2}\int d^3\mathbf{r}d^3\mathbf{r}'\frac{1-3(\hat{e}\cdot\hat{u}_B)^2}{|\mathbf{r}-\mathbf{r}'|^3}\Big[\frac{1}{2}\Big(S^X(\mathbf{r})S^X(\mathbf{r}')+S^Y(\mathbf{r})S^Y(\mathbf{r}')\Big)\\
&-S^Z(\mathbf{r})S^Z(\mathbf{r}')\Big]-i\int d^3\mathbf{r}\sum_{l,m}\beta_{l,m}\,|\Psi_m(\mathbf{r})|^2\,|\Psi_l(\mathbf{r})|^2 \qquad (1)
\end{aligned}
$$

The spin density vector is $\mathbf{S}(\mathbf{r})=\boldsymbol{\Psi}^\dagger(\mathbf{r})\cdot\mathbf{s}\cdot\boldsymbol{\Psi}(\mathbf{r})$ with $\mathbf{s}=\{s^X,s^Y,s^Z\}$ spin-3 matrices. $\hat{H}_0=-\frac{\hbar^2}{2M}\nabla^2+V_{\rm trap}(\mathbf{r})$ is the single particle Hamiltonian, with $V_{\rm trap}(\mathbf{r})$ the spin-independent harmonic trapping potential.

The term proportional to c_0 describes the contact density interaction, with $n(\mathbf{r})=\boldsymbol{\Psi}^\dagger(\mathbf{r})\cdot\boldsymbol{\Psi}(\mathbf{r})$ the condensate density. The terms proportional to c_1,c_2,c_3 describe the contact spin dependent interactions [16], with $A_{SM_S}(\boldsymbol{r})=\sum_{mm'=-3}^{3}\langle S,M_S|3,m;3,m'\rangle\,\Psi_m(\boldsymbol{r})\Psi_{m'}(\boldsymbol{r})$. For ^{52}Cr, we use $c_0=71\ g_c a_B$, $c_1=3.5\ g_c a_B$; $c_2=-15.5\ g_c a_B$, $c_3=-46.5\ g_c a_B$, with $g_c=4\pi\hbar^2/M$, and a_B the Bohr radius [15, 17, 18].

The term proportional to $c_{dd}=\mu_0(g\mu_B)^2/(4\pi)$ (with μ_0 the magnetic permeability of vacuum, and $\hat{e}=(\mathbf{r}-\mathbf{r}')/|\mathbf{r}-\mathbf{r}'|$) is the secular Hamiltonian of DDIs which conserves magnetization along the magnetic field. Magnetization non-conserving terms of DDIs give rise to the observed atom losses, which we take into account by adding the imaginary term $i\Gamma$, following [19].

$\hat{H}_0$ can be enriched by a quadratic term $q(S^Z)^2$; for Cr, it corresponds to the (small) tensorial light shift induced by the 1075 nm laser creating the optical trap. We show in Fig. 3 that $q\simeq6$ Hz leads to slightly better agreement with the data; it can account as well for the small dynamics of Fig. 2a).

The GP simulations compare well to experimental data (see Figs. 2, 3), with no adjustable parameter ($q=0$). Simulations thus allow us to probe the relative influence of the different interactions. We show on

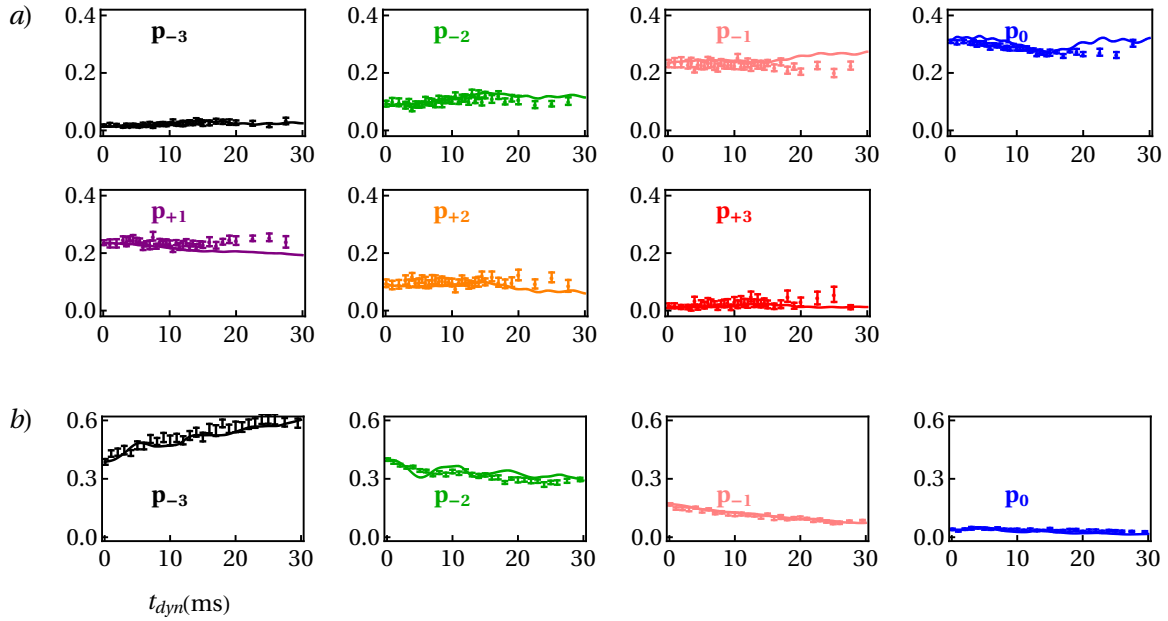

FIG. 2. Temporal evolutions for $B_0 = 189$ mG, $\hat{u}_B = \cos(34 \times \pi/180)\,\hat{u}_x + \sin(34 \times \pi/180)\,\hat{u}_z$, $(b_x, b_y, b_z) = (3.5 \pm 15, 3.6 \pm 7, 1.8 \pm 17)$ mG.cm^{-1}. a) $\theta = \pi/2$. b) $\theta = \pi/4$. We show experimental data (points) and result of our Gross Pitaevskii simulations without free parameters (solid line), for the seven fractional populations in a), and in b) for the 4 fractional populations significantly populated. Error bars take into account both statistical and systematics uncertainties.

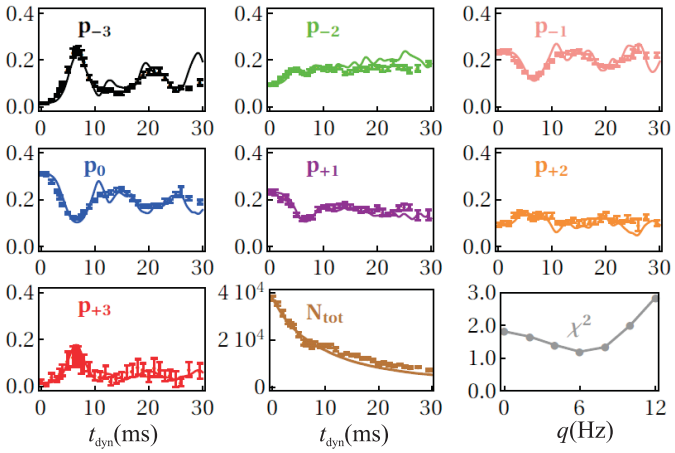

FIG. 3. Temporal evolution following an initial rotation by an angle $\theta = \pi/2$, for $B_0 = 170$ mG, $\hat{u}_B = \hat{u}_z$, $(b_x, b_y, b_z) = (1.6 \pm 7, 44.6 \pm 7, 5.7 \pm 8)$ mG.cm^{-1}. We show experimental data (points) and results of Gross Pitaevskii simulations (full lines), for the seven fractional populations, and for the total number of atoms (bottom center). Error bars take into account both statistical and systematics uncertainties. Bottom right: influence of a non zero quadratic effect. The χ^2 criteria, evaluated over the full spin populations data, is plotted as a function of q.

Fig. 4a) what is the expected dynamics if DDIs or contact spin dependent interactions are neglected (setting $a_0 = a_2 = a_4 = a_6 = (9a_4 + 2a_6)_{\rm real}/11$). The striking differences seen for the different cases show the prominent role played by contact spin exchange processes. In this example $\theta = \pi/2$, but even in the case of $\theta = \pi/4$, where DDIs are instrumental in triggering spin dynamics (see Fig. 2b)), similar conclusions hold.

Furthermore, simulations confirm that in presence of small MGs spin mixing develops for $\theta = \pi/4$ (see Fig. 2 b)); and that, on the contrary, spin mixing dynamics is much reduced for $\theta = \pi/2$ (see Fig. 2 a)), unless a MG is applied (see Fig. 3). This was discussed in [8] for the particular case $\boldsymbol{b}//\hat{u}_B$; our simulations indicate that MGs with $\boldsymbol{b} \perp \hat{u}_B$ are even more efficient to trigger dynamics. Therefore MGs play a key role to trigger spin mixing dynamics in our system (as opposed to e.g. [20], where MGs can suppress spin exchange processes).

Just after rotation, all spins are maximally stretched (and aligned), so that the sample is ferromagnetic. One striking observation in our simulations is that a ferromagnetic character is maintained while dynamics proceeds. We investigate this property by computing the local spin length $\Pi(\mathbf{r}) = |\mathbf{S}(\mathbf{r})|/n(\mathbf{r})$ $(0 \leq \Pi(\mathbf{r}) \leq 3)$ integrated over the cloud, which is maximal for a ferromagnetic state. We find that the integrated spin length remains close to 3 (see Fig. 4b)) during dynamics. This protection of ferromagnetism, which would be even more pronounced in absence of DDIs (see Fig.4 b)), comes as a surprise since $a_6 > a_4$ energetically disfavors ferromagnetism in the ^{52}Cr BEC [21].

To understand this effect, we have solved the GP equation for a homogeneous BEC in presence of MGs. We find that the initial ferromagnetic character of the BEC is protected by spin exchange contact interactions, which provide self-locking of the spinor components, similar to the one observed in atomic clocks [22]. Such locking occurs because the initial spinor state lies at an extremum

(for us a maximum) in energy. On the other hand, phase scrambling between the different m_s components arises due to increasing kinetic energy associated to acceleration by MG. For a homogeneous gas of density n after an evolution time T, and provided incoherent scattering remains negligible [23], ferromagnetic protection is ensured if $(m_s g\mu_B b)^2 T^2/(2M) << c_1 n$ [24]. This criterion, which can also be derived from a linear response theory (see Appendix), highlights the crucial role of the energy mismatch set by c_1 (further investigated in Appendix). In a trap the criterion is set by the ratio between maximal kinetic energy (corresponding to $T = \pi/(2\omega)$) and $c_1 n$, which is equal to about 0.05 in our case.

Taking the phenomenological assumption that the local spinor remains ferromagnetic, we derived the following evolution of the fractional populations (see Appendix) after a $\pi/2$ pulse, assuming that the system is described by the ferromagnetic hydrodynamics equations [25] (which underlines a connection to the physics of ferrofluids), and taking an initial Gaussian ansatz of $1/e^2$ radius R:

$$\frac{p_{m_s}(t)}{p_{m_s}(0)} = 1 + \frac{1}{2}\left(\frac{g\mu_B b}{MR}\right)^2 \left(m_s^2 - \sum_{m_{s'}} m_{s'}^2 p_{m'_s}(0)\right) t^4 \quad (2)$$

Thus a state can remain ferromagnetic only if spin exchange processes counterbalance the change in local populations due to the separation between spin components induced by MGs. We find excellent agreement of this surprisingly simple equation with simulations at short time when only contact interactions are taken into account (see Fig. 4a), and Appendix). We stress that this equation is independent of interactions, which are in practice adiabatically eliminated. Large enough spin-dependent interactions thus convey metastability to ferromagnetism and lead to a universal behavior, whether the spinor ground state is ferromagnetic, or not (e.g. ^{52}Cr is expected to have a cyclic ground state [18]). This finding is the second main result of our paper.

To confirm the persistence of ferromagnetism, we performed experiments where we applied a second $\pi/2$ rf pulse with a random phase of the rf field, just before Stern-Gerlach projection. We then measure the absolute value of the normalized magnetization, $|\sum m_s p_{m_s}|$. The envelop of the fluctuating data provides a lower-range value for the norm of the collective spin $L = \left|\int d^3\mathbf{r}\mathbf{S}(\mathbf{r})\right|/N$ (see e.g. [26], and Appendix). Experimental results, shown in Fig. 4c), are thus in very good agreement with numerical simulations for L. Unlike $\Pi(\mathbf{r})$, L significantly departs from 3: this indicates that while the spins remain (almost) locally polarized, spin textures grow, mostly corresponding to $\mathbf{S}(\mathbf{r})$ pointing along different directions in different parts of the BEC. On the other hand, the fact that L reaches a value close to the initial

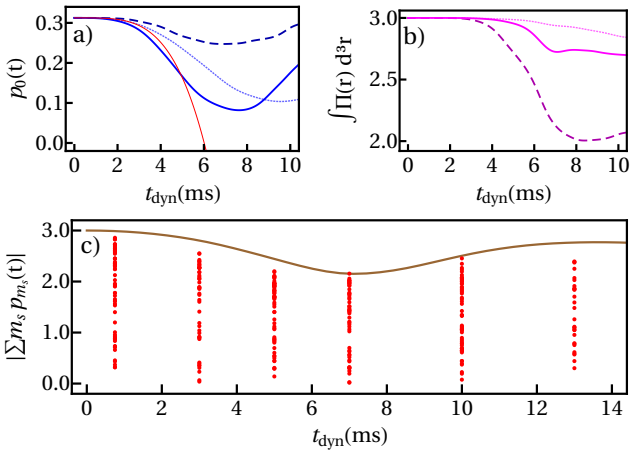

FIG. 4. Top: results of numerical simulations for the magnetic field configuration of Fig. 3. We compare the real case (thick full lines) to the case where contact spin dependent (dashed lines) or dipolar interactions (dotted lines) are suppressed (see text). a): fractional populations in $m_s = 0$. The (red) thin line corresponds to our model at short time (see eq.(2)). b): spin length integrated over all cloud. Bottom: measurement of the norm of the collective spin, L. Circles are the measured values of $|\sum m_s p_{m_s}|$ after a $\pi/2 - t - \pi/2$ sequence, while the full line is the value of L, obtained from our GP simulations.

one at $t_{\rm dyn} = 10 - 13$ ms is an experimental proof that the spins are then almost in a stretched state, and almost parallel.

Our GP simulations confirm this scenario, and the appearance of spin textures (see Fig. 1b)). However, in contrast to [8], in situ spin structures are strongly modified after time of flight in our case, and their study goes beyond the scope of this paper. In our experiment, spin textures of dipolar origin can be created at a rate of order [13] $\Gamma_{dd} = (3nc_{\rm dd})/\hbar = 2.5 \times 10^2$ s^{-1}, with $n = 2.5 \times 10^{20}$m^{-3}. On the other hand, the relevant spin exchange rate reads $\Gamma_{4,6} = 4\pi\hbar n(a_6 - a_4)/(11M) = 7 \times 10^2$ s^{-1}. These estimates show the interplay between contact and dipolar interactions for the appearance of spin textures.

In conclusion, we have investigated the spin mixing dynamics for a $s = 3$ spinor BEC following a rotation of the individual spins, initially aligned along the magnetic field. We have observed that while DDIs can trigger dynamics for $\theta \neq \pi/2$, MGs are necessary for $\theta = \pi/2$. For this case, we have demonstrated the occurrence of an original scenario, in which strong spin dependent interactions drive the dynamics as a response to MGs, and tend to lock the spinor onto a ferromagnetic state, even though depolarization is energetically favoured. Unfortunately this scenario seems to disfavour appearance of beyond mean field effects in our system, which by contrast would reduce the local spin length. Our configuration is thus probably at the limit of seeing beyond mean-field physics, which could for example be enhanced by working in lower dimensions.

Acknowledgements: We thank O. Gorceix and E. Maréchal for important contributions enabling this

work, and M. Robert de Saint Vincent for stimulating discussions. The Villetaneuse group acknowledges financial support from Conseil Régional d'Ile-de-France under DIM Nano-K / IFRAF, CNRS, Ministère de l'Enseignement Supérieur et de la Recherche within CPER Contract, Université Sorbonne Paris Cité (USPC), and the Indo-French Centre for the Promotion of Advanced Research - CEFIPRA under LORIC5404-1 and PPKC contracts. AMR acknowledges support by Defense Advanced Research Projects Agency (DARPA, W911NF-16-1-0576 through ARO), NSF grant PHY 1521080, JILA-NSF grant PFC-1125844, the Air Force Office of Scientific Research and its Multidisciplinary University Research Initiative (AFOSR-MURI).

APPENDIX

In this Appendix, we give experimental details concerning the Stern-Gerlach (SG) procedure, the measurement of magnetic field gradients, the calibration of spin detection measurement, and the measurement of the norm of the collective spin. We also discuss why spin exchange interactions provide a feedback mechanism which tends to maintain the ferromagnetic character of the spins during spin dynamics. We show from our Gross-Pitaevskii simulations that conservation of ferromagnetism is provided by spin-dependent interactions corresponding to the term c_1. We finally provide two models to explain the role of magnetic gradients in the spin dynamics, a basic one, and one based on an hydrodynamic approach, which both allow to retrieve equation (2). Supplemental experimental data is also provided.

Stern Gerlach procedure

The SG field is in the horizontal plane along a direction x', and has the form: $\vec{B}_{SG} = (B_{SG} + bx')\,\vec{u}_{x'}$, with $b \approx 0.5$ G.cm^{-1}. Atoms in different spin states are separated by the associated spin-dependent force. After $t_{TOF} = 5$ ms of free fall in presence of the gradient, atoms are imaged through standard absorption imaging, with a 425 nm resonant circularly polarized laser beam. The value of t_{TOF} was chosen in order to have sufficient spatial separation between spin components, while maintaining good signal to noise ratio for imaging (see Fig 1 c)d) of the main article).

Measurement of magnetic field gradients

To measure the magnetic field gradient during spin dynamics, we proceed to a differential measurement, consisting in measuring the ballistic expansion of a BEC prepared for two different m_s states. We let the cloud expand in $\vec{B}_{dyn}$ for 10 ms. We compare the final position of atoms initially in $m_s = 3$ with that of atoms initially in $m_s = -3$, by applying or not a frequency sweep across the Larmor frequency f_L before expansion. For $\vec{B}_{dyn} = (B_0 + \alpha x + \beta y + \gamma z)\,\vec{u}_B + B_1\vec{u}_\perp$, with $\{\alpha x, \beta y, \gamma z, B_1\} \ll B_0$ in the entire cloud, $\left|\vec{B}\right| \simeq B_0 + \alpha x + \beta y + \gamma z$, so that the force experienced by the atom is $g m_S \mu_B\,(\alpha\vec{u}_x + \beta\vec{u}_y + \gamma\vec{u}_z)$. To measure α, β and γ, we take absorption images along two approximately orthogonal directions.

Calibration of imaging system

The raw values of the populations of the spin components obtained by integration of absorption images do not give absolute values of the populations. This can be for example inferred from the picture shown in Fig. 1 c). The initial rotation $\theta = \pi/2$ is then expected to lead to a symmetric population distribution ($N_{m_s} = N_{-m_s}$), but in Fig. 1 c), there is a growing deficit in population with m_s, so that in particular N_{+3} is substantially undervalued.

This systematic effect mostly derives from the fact that the cross section for absorption of resonant light strongly depends on the m_s states, through Clebsch-Gordan coefficients. First, the magnetic field during imaging is not parallel to the imaging beam axis. Second, optical pumping by the imaging beam is not fast enough compared to the 75 μs duration of the imaging pulse, on the 425 nm $J \to J+1$ transition, with an intensity of 0.04 the saturation intensity.

Calibration of normalization factors f_{m_s}, with $N_{m_s} = f_{m_s} N_{m_s,raw}$, are obtained by comparing measured populations following immediately rotations of $\theta = \pi/4, \pi/2, 3\pi/4$, and π, with theoretically expected values. This calibration depends on the magnetic field direction during spin dynamics, as eddy currents do not allow to rapidly set the direction of the magnetic field during imaging. For example for the data in Fig. 3 of the main article: $f_{-3} = 1 \pm 0.15$, $f_{-2} = 1 \pm 0.1$, $f_{-1} = 1.4 \pm 0.15$, $f_0 = 2.25 \pm 0.2$, $f_{+1} = 4.35 \pm 0.45$, $f_{+2} = 5.4 \pm 0.2$, $f_{+3} = 6 \pm 2$. Error bars in this calibration are used to compute systematic errors on relative populations.

Norm of the collective spin

In the case $\theta = \pi/2$, our GP simulations show a persistence of the local ferromagnetic character of the ^{52}Cr BEC. Experimentally, we cannot measure local quantities such as local spin length: we have only access to collective quantities. In particular, we can measure the norm of the collective spin, normalized to the atom number, that we note L. The maximum of L is 3 (as we deal with spin 3 atoms), and is only obtained in the case of a ferromagnetic sample with all spins aligned (e.g. the initial state in our experiment). On the other hand the minimum of L, 0, can be reached even with a ferromagnetic sample, when all spins are in a stretched state but point along random directions; or if all atoms are prepared in $m_s = 0$.

The measurement of L provides an other comparison between experiment and our GP simulations. Besides, a large value of L (close to 3) is only compatible with a ferromagnetic sample: measuring L close to 3 after the spin dynamics has processed demonstrate that the ferromagnetic character of the gas is preserved (see Fig.4 c) of the main article).

To measure L at a given time $t_{\rm dyn}$ of the spin dynamics, we use a second $\pi/2$ RF pulse at $t_{\rm dyn}$. As the first RF pulse, it induces a rotation of all spins by $\pi/2$ around the Oy axis, while the external B field is along Oz. Because of a jitter of the Larmor frequency during the dynamics, the direction of the collective spin just before the second RF pulse is random in the Oxy plane for $t_{\rm dyn} > 1$ ms. We then measure populations in the z basis with our SG analysis. The quantity $|\sum m_s p_{m_s}|$ will range from 0 to L, depending if the collective spin just before the second RF pulse points along Oy or Ox. To evaluate the value of L we therefore repeat the measurement a large number of times (50 for the data of Fig. 4c)) and the maximal value of $|\sum m_s p_{m_s}|$ is a lower-range value for L.

Interaction-driven ferromagnetic protection in an homogeneous gas

One of the surprising features revealed by the numerical simulations is that, in the presence of a magnetic field gradient, spin dynamics takes place *while preserving the local ferromagnetic character* of the spinor order parameter. Here we present a short derivation of the conditions for the ferromagnetic protection for an homogeneous spinor BEC gas. The results are derived from a linear response analysis of the Gross-Pitaevskii equation (GPE). For simplicity we set to zero all subleading spin dependent interactions and only keep c_1 (direct exchange) i.e. $c_2 = c_3 = c_{dd} = 0$. We also set $V_{\rm trap} = 0$ and $B_0 = 0$. The latter is because the constant part of the magnetic field can be factored out and does not play a role in the dynamics. The initial condition is a ferromagnetic state along the x direction which we denote as $\Psi_m(x, t = 0) = n\langle m| - s_x\rangle$. The exact dynamics generated by the GPE is rather complex. However, its short-time limit can be captured quite easily when b is small by postulating a solution of the form :

$$\Psi_m(x,t) = \sqrt{n}\,\mathrm{e}^{-\mathrm{i}\,\mu t}[\langle m| - s_x\rangle + z_m(x,t)],$$

with $\mu = \big(c_0 + s^2 c_1\big)n$ and $|z_m| \ll 1$ (z_m is complex and depends only on x), and expand non-linear terms in the GPE in powers of z_m. After some straightforward algebra we arrive at the time-dependent fractional populations:

$$\frac{p_m(t)}{p_m(0)} = 1 + \frac{\hbar^2(g\mu_B b)^2}{2M\nu^3}\zeta(\tau)\Big[m^2 - \sum\nolimits_n n^2 p_n(0)\Big]$$

with $\zeta(\tau) = [\tau^2 - \sin^2\tau]$, $\tau = \nu t/\hbar$ and $\nu = c_1 sn$. For times $t < \hbar/c_1 n$, spin dynamics occurs, with a population change $\propto c_1 n$. For large enough spin-dependent interactions, corresponding to $\beta = \frac{\hbar^2(g\mu_B b)^2}{M\nu^3} \to 0$, this corresponds to a very small change in populations, which can be in practice neglected. In our experiment, $\beta < 10^{-6}$. For times $t > \hbar/c_1 n$, while still considering the perturbative regime valid, we only need to keep the quadratic term in ζ ($\tau^2 \gg \sin^2\tau$) and the populations remain locked in a ferromagnetic state when $(g\mu_B b)^2 t^2/[M(c_1 sn)] << 1$. This condition (also given in the main part) insures that no population dynamics occurs *for a homogeneous gas* and that the gas remains ferromagnetic.

Effect of the different spin-dependent contact interaction terms

We have performed a systematic study with our Gross-Pitaevskii simulation, where we vary the different spin-dependent interaction terms $c_{1,2,3}$. We consider four different cases. The first case corresponds to all spin-dependent interactions canceled. The second case is when only c_1 is kept non zero. The third case is when only c_2 is kept non zero. The fourth case is when only c_3 is kept non zero. Coefficients c_i are set by the numerical values of the 4 scattering lengthes of ^{52}Cr coming into play ([16]): $a_{0,2,4,6}$. To ensure relevant comparison, we start for all cases from the same fully polarized initial state, entirely defined by the value of a_6: for all cases the numerical value of a_6 is the real one. We then vary the numerical values of $a_{0,2,4}$ to obtain the desired value of c_i. For example in the first case we set $a_0 = a_2 = a_4 = a_6$.

We plot in Fig. 5 the fractional populations, and the integrated spin length as a function of time, for these different cases. We find that, while any of the $c_{1,2,3}$ by itself can drive spin dynamics, the local ferromagnetic character of the gas is only preserved when c_1 is non

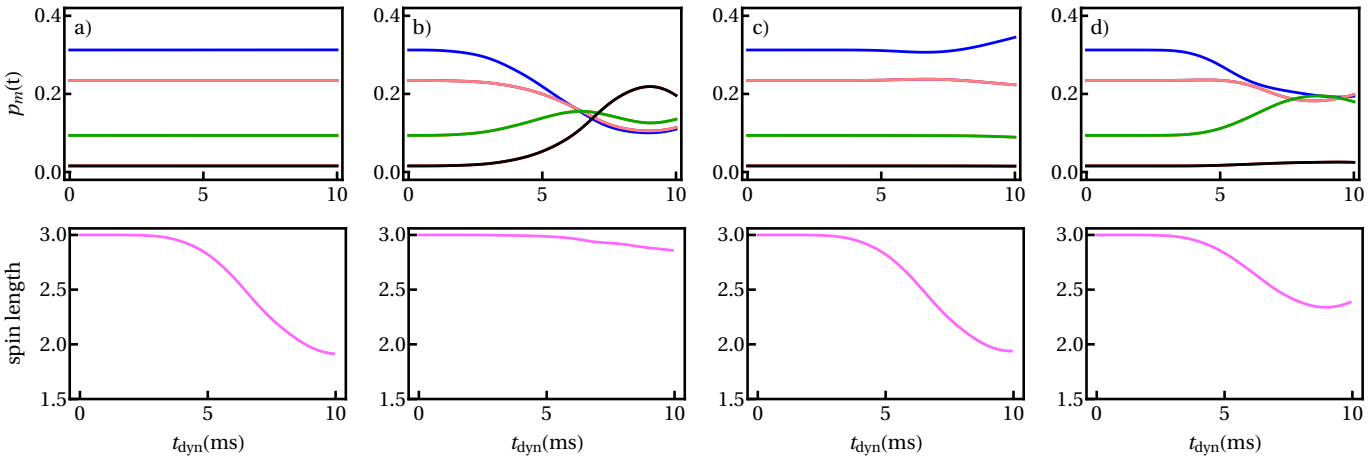

FIG. 5. Results of our Gross-Pitaevskii simulation without DDIs, for the experimental conditions of Fig. 3). We keep the same initial (fully polarized) ground state, and set some of the spin dependent interactions terms $c_{1,2,3}$ to 0. Top: fractional populations, corresponding from top to bottom at $t = 0$ to p_0, $p_{\pm1}$, $p_{\pm2}$, $p_{\pm3}$. Bottom: spin length integrated over all cloud. a): $c_1 = c_2 = c_3 = 0$, b): $c_2 = c_3 = 0$, c): $c_1 = c_3 = 0$, d): $c_1 = c_2 = 0$.

vanishing. This confirms the crucial impact of the energy mismatch $c_1 n$ to preserve ferromagnetism.

A physical interpretation of this result is the following. Atoms are initially in state $m_s = -3$ along the Ox axis, which first couples to state $m_s = -2$ through MGs. The $m_s = -2$ state involve collisions only in the molecular channels $S = 6$ and $S = 4$. Therefore, the molecular channels $S = 2$ and $S = 0$ do not come into play at the earlier stage of the dynamics, hence the leading role of c_1 compared to $c_{2,3}$ which involve $a_{0,2}$ (see [16]).

Basic derivation of equation (2)

In this paragraph we provide a basic derivation of equation 2 describing perturbative population dynamics in the limit of very fast spin exchange dynamics. We consider a spinor BEC with a spin equal to s, initially in a ferromagnetic state, characterized by initial fractional populations $p_{m_s,i}$. For $t > 0$, a magnetic gradient b imparts differential accelerations a_{m_s} to the different m_s states: $a_{m_s} = m_s a$, with $a = g\mu_B b/M$.

At $t = 0$, all atomic distributions are the same. At a given time $t > 0$ atomic distributions of the different m_s states are translated by $x_{m_s}(t) = \frac{1}{2} a_{m_s} t^2$. In this basic approach we consider that population of a given m_s state is split in two. First, the part which has moved away from the initial volume occupied by the atoms (with corresponding population $N_{m_s,ext}$), which does not experience spin mixing. And second, the part which is still in this initial volume (with corresponding population $N_{m_s,c}$). We therefore obtain the following decomposition for the population of all m_s states:

$$N_{m_s,i} = N_{m_s,ext} + N_{m_s,c} \tag{3}$$

At short times we have:

$$N_{m_s,c} = N_{m_s,i}\left(1 - \frac{x_{m_s}(t)^2}{W^2}\right) \tag{4}$$

where W is the typical spatial extension of the cloud.

The populations in the inner part are modified by spin mixing such that, after mixing has taken place, the ferromagnetic character is recovered; we note the corresponding populations $N_{m_s,c,f}$. For $\theta = \pi/2$, transport associated to MGs preserve locally the initial magnetization (0), and the condition to recover ferromagnetism is:

$$\frac{N_{m_s,c,f}}{N_{c,tot}} = p_{m_s,i} \tag{5}$$

with $N_{c,tot} = \sum_{m_s} N_{m_s,c}$. After spin dynamics the total spin population in a given m_s state, $N_{m_s,f}$, is given by $N_{m_s,f} = N_{m_s,ext} + N_{m_s,c,f}$, and consequently the final fractional populations are given by:

$$p_{m_s}(t) = p_{m_s,f} = p_{m_s,i}\frac{x_{m_s}(t)^2}{W^2}$$
$$+p_{m_s,i}\sum_{m_{s'}} p_{m_{s'},i}\left(1 - \frac{x_{m_{s'}}(t)^2}{W^2}\right) \tag{6}$$

which gives:

$$\frac{p_{m_s}(t)}{p_{m_s,i}} = 1 + \left(\frac{g\mu_B b}{2MW}\right)^2\left(m_s^2 - \sum_{m_{s'}} m_{s'}^2 p_{m_{s'},i}\right)t^4 \tag{7}$$

This simple approach qualitatively yields the good result of eq. (2). Below, integration over the spatial distributions is done exactly.

Hydrodynamic approach

The metastability of the ferromagnetic character of the gas, justified above, provides a way to considerably simplify the theoretical treatment. We phenomenologically *assume* that the BEC always remains locally ferromagnetic, which allows us to derive hydrodynamic equations, which are equivalent to the ferromagnetic Gross-Pitaevskii equation. For a fully polarized BEC, one can find dynamics equations for the density ρ, mass velocity $\boldsymbol{v}^{\text{mass}}$, spin velocity $\boldsymbol{v}_\mu^{\text{spin}}$ and for the spin density $\mathbf{F}$ of component $\mathcal{F}_\mu$ [16]. In the following, the dipolar interaction is neglected. The equation for $\mathcal{F}_\mu$ then reads:

$$\frac{\partial \mathcal{F}_\mu}{\partial t} + \nabla.\left[\rho \boldsymbol{v}_\mu^{\text{spin}}\right] = \frac{g\mu_B}{\hbar}\left(\mathbf{B}_{dyn} \times \mathbf{F}\right)_\mu \qquad (8)$$

where $\mu = (x, y, z)$, g is the Landé factor, μ_B the Bohr magneton, and $\mathbf{B}_{dyn}$ the (inhomogeneous) magnetic field. We define the local spin density $\boldsymbol{f} = \mathbf{F}/\rho$ and we suppose that $\boldsymbol{v}^{\text{mass}} \sim 0$ therefore $\frac{\partial \rho}{\partial t} = -\nabla.\left[\rho \boldsymbol{v}^{\text{mass}}\right] \sim 0$ (in accordance with our full numerical simulations of the Gross-Pitaevskii equation). Then Eq.(8) becomes:

$$\rho\frac{\partial f_\mu}{\partial t} + \nabla.\left[\rho \boldsymbol{v}_\mu^{\text{spin}}\right] = \frac{g\mu_B\rho}{\hbar}\left(\mathbf{B}_{dyn} \times \mathbf{f}\right)_\mu \qquad (9)$$

where

$$\begin{aligned} \boldsymbol{v}_x^{\text{spin}} &= -\tfrac{\hbar}{2Ms}\left(f_y\nabla f_z - f_z\nabla f_y\right) \qquad (10)\\ \boldsymbol{v}_y^{\text{spin}} &= -\tfrac{\hbar}{2Ms}\left(f_z\nabla f_x - f_x\nabla f_z\right)\\ \boldsymbol{v}_z^{\text{spin}} &= -\tfrac{\hbar}{2Ms}\left(f_x\nabla f_y - f_y\nabla f_x\right) \end{aligned}$$

where s is the spin ($s = 3$ in our case); M is the mass.

Starting from a fully polarized BEC we rotate the spins around the Oy axis with an angle θ. In the presence of an inhomogeneous magnetic field $\mathbf{B}_{dyn} = g\mu_B B_0 \boldsymbol{e}_z + g\mu_B bx\boldsymbol{e}_z$, the spin precess around $\boldsymbol{e}_z$ (in addition to the homogeneous Larmor precession at frequency $\omega_L = g\mu_b B_0 x/\hbar$ which factors out of the problem) with a frequency $\omega_b = g\mu_B bx/\hbar$. We used a Gaussian ansatz for the density $\rho = \frac{N}{\left(\frac{\pi}{2}\right)^{3/2}R^3}\exp\left[-2\boldsymbol{r}^2/R^2\right]$, with N he number of atoms and R the size of the cloud. We then recover eq. (2).

In Fig. 6, we plot the result of eq.(2) alongside our numerical simulations of the Gross-Pitaevskii equation without dipole-dipole interactions for the different fractional populations in states m_s. The agreement is remarkable, confirming the validity of the ferromagnetic approximation and the hydrodynamic approach.

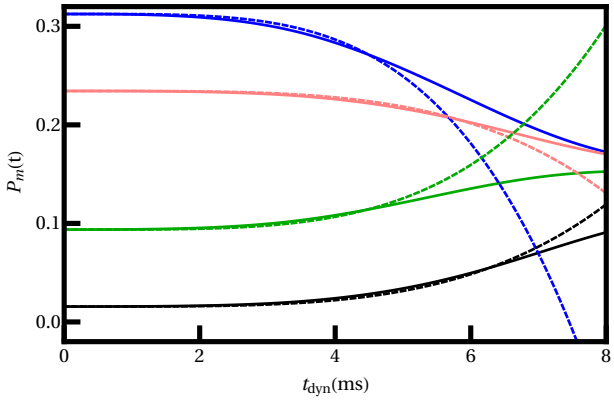

FIG. 6. Comparison between our perturbative ferromagnetic model to fourth order, and the full numerical simulation of the Gross-Pitaevskii equation. Populations as a function of time, corresponding from top to bottom at $t = 0$ to p_0, $p_{\pm1}$, $p_{\pm2}$, $p_{\pm3}$. The trap is spherical with a trap frequency of 320 Hz, the atom number is 30 000, and the magnetic gradient is equal to 3.5 mG.cm^{-1}.

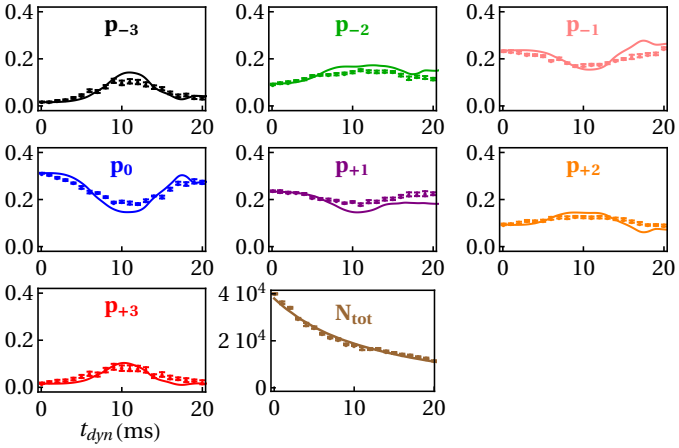

FIG. 7. Data for smaller gradient than in Figure 3. $B_0 = 176$ mG, $\vec{u}_B = \vec{u}_x$, $(b_x, b_y, b_z) = (0 \pm 10, 7 \pm 7, 19.6 \pm 10)$ mG.cm^{-1}. Full lines are result of our simulations with no adjustable parameters.

Supplemental data

We plot in Fig. 7 supplemental data, showing the evolution of p_{m_s} for $\theta = \pi/2$ and a $\mathbf{B}_{dyn}$ configuration different than the ones in Fig. 2 a) and Fig. 3. The agreement between experimental data and numerical simulations is as good as in these Figures, confirming the validity of our numerical simulations. We find again that the data exhibit spin dynamics over the timescale $\left(\frac{2MR}{g\mu_B b}\right)^{1/2}$ given by eq. (2).

[1] Principles of nuclear magnetism, A. Abragam, Oxford Science Publications

[2] J. S. Waugh, L. M. Huber, and U. Haeberlen, Phys. Rev. Lett. **20**, 180 (1968)

[3] A. M. Tyryshkin, S. Tojo, J.J.L. Morton, H. Riemann, N.V. Abrosimov, P. Becker, H.J. Pohl, T. Schenkel,

M.L.W. Thewalt, K. M. Itoh and S. A. Lyon, Nature Materials **11**, 143 (2012)
[4] R. Hanson and D.D. Awschalom, Nature **453**, 1043 (2008)
[5] B. Yan, S.A. Moses, B. Gadway, J.P. Covey, K.R.A. Hazzard, A. M. Rey, D.S. Jin and J. Ye, *Nature* **501**, 521 (2013)
[6] D M. Stamper-Kurn and M. Ueda, Rev. Mod. Phys. **85**, 1191 (2013)
[7] M. Vengalattore, S. R. Leslie, J. Guzman and D. M. Stamper-Kurn Phys. Rev. Lett. **100**, 170403 (2008)
[8] Y. Eto, H. Saito and T. Hirano Phys. Rev. Lett. **112**, 185301 (2014)
[9] J. Kronjäger, C. Becker, P. Soltan-Panahi, K. Bongs and K. Sengstock Phys. Rev. Lett. **105**, 090402 (2010)
[10] K. R. A. Hazzard, S. R. Manmana, M. Foss-Feig and A. M. Rey Phys. Rev. Lett. **110**, 075301 (2013)
[11] B. Naylor, M. Brewczyk, M. Gajda, O. Gorceix, E. Maréchal, L. Vernac, and B. Laburthe-Tolra Phys. Rev. Lett. **117**, 185302 (2016)
[12] A. de Paz, P. Pedri, A. Sharma, M. Efremov, B. Naylor, O. Gorceix, E. Maréchal, L. Vernac, and B. Laburthe-Tolra, Phys. Rev. A **93**, 021603(R) (2016)
[13] Y. Kawaguchi, H. Saito and M. Ueda, Phys. Rev. Lett. **98**, 110406 (2007)
[14] P. Blakie, A. Bradley, M. Davis, R. Ballagh, and C. Gardiner, Advances in Physics **57**, 363 (2008)
[15] B. Pasquiou, G. Bismut, Q. Beaufils, A. Crubellier, E. Maréchal, P. Pedri, L. Vernac, O. Gorceix, and B. Laburthe-Tolra, Phys. Rev. A **81**, 042716 (2010)
[16] Y. Kawaguchi and M. Ueda, Phys. Rep. **520**, 253 (2012)
[17] J. Werner, A. Griesmaier, S. Hensler, J. Stuhler, T. Pfau, A. Simoni, and E. Tiesinga, Phys. Rev. Lett. **94**, 183201 (2005)
[18] A. de Paz, B. Naylor, J. Huckans, A. Carrance, O. Gorceix, E. Maréchal, P. Pedri, B. Laburthe-Tolra, and L. Vernac, Phys. Rev. A **90**, 043607 (2014)
[19] C.G. Pethick and H. Smith, Bose Einstein Condensation in dilute gases, Cambridge University Press.
[20] F. Deuretzbacher, G. Gebreyesus, O. Topic, M. Scherer, B. Lücke, W. Ertmer, J. Arlt, C. Klempt, and L. Santos, Phys. Rev. A **82**, 053608 (2010)
[21] B. Pasquiou, E. Maréchal, G. Bismut, P. Pedri, L. Vernac, O. Gorceix, and B. Laburthe-Tolra, Phys. Rev. Lett. **106**, 255303 (2011)
[22] C. Deutsch, F. Ramirez-Martinez, C. Lacroûte, F. Reinhard, T. Schneider, J. N. Fuchs, F. Piéchon, F. Laloë, J. Reichel, and P. Rosenbusch, Phys. Rev. Lett. **105**, 020401 (2010)
[23] F. Piéchon, J. N. Fuchs, and F. Laloë, Phys. Rev. Lett. **102**, 215301 (2009)
[24] One can adapt this criterion to spin 1 or 2 BECs using [16].
[25] K. Kudo and Y. Kawaguchi, Phys. Rev. A **82**, 053614 (2010)
[26] Y. Eto, M. Sadgrove, S. Hasegawa, H. Saito, and T. Hirano, Phys. Rev. A **90**, 013626 (2014)